Electrochemical behaviour of TiO_xC_y as catalyst support for direct ethanol fuel cells at intermediate temperature: from planar systems to powders

Laura Calvillo,[†] Gonzalo García,[‡] Andrea Paduano,[Δ] Olmedo Guillen-Villafuerte,[‡] Carlos Valero-Vidal,[◊,§] Andrea Vittadini,[•] Marco Bellini,[⊥] Alessandro Lavacchi,[⊥] Stefano Agnoli,[†] Alessandro Martucci,[Δ] Julia Kunze- Liebhäuser,[◊] Elena Pastor[‡] and Gaetano Granozzi [†,]*

[†] Department of Chemical Sciences, University of Padova, Via Marzolo 1, 35131 Padova, Italy

[‡] Instituto Universitario de Materiales y Nanotecnología, Universidad de La Laguna, Astrofísico F. Sánchez s/n, 38071 La Laguna, Tenerife, Spain.

[Δ] Department of Industrial Engineering, Via Marzolo 9, 35131 Padova, Italy

[◊] Leopold-Franzens-University Innsbruck, Institute of Physical Chemistry, Innrain 52c, Innsbruck, 6020 Austria

[•] CNR-IENI, Via Marzolo 1, 35131 Padova, Italy

[⊥] CNR-ICCOM, Via Madonna del Piano, 10, 50019 - Sesto Fiorentino (FI)

KEYWORDS. Titanium oxycarbide, support, DEFCs, intermediate-T, electrochemical stability.

ABSTRACT. In order to achieve complete oxidation of ethanol (EOR) to CO_2, higher operating temperatures (often called intermediate-T, 150 – 200 °C) and appropriate catalysts are required. We examine here titanium oxycarbide, (hereafter TiO_xC_y), as a possible alternative to standard carbon based supports to enhance the stability of the catalyst/support assembly at intermediate-T. In order to test this material as electrocatalyst support, a systematic study of its behavior under electrochemical conditions was carried out. To have a clear description of the chemical changes of TiO_xC_y induced by electrochemical polarization of the material, a special set-up which allows to combine X-ray photoelectron spectroscopy and electrochemical measurements was used. Subsequently, an electrochemical study was performed on TiO_xC_y powders, both at room temperature and at 150 °C. The present study has revealed that TiO_xC_y is a sufficiently conductive material whose surface is passivated by a TiO_2 film under working conditions, which prevents the full oxidation of the TiO_xC_y, and which can thus be considered a stable electrode material for EOR working conditions. This result has also been confirmed through density functional theory (DFT) calculations on a simplified model system. Furthermore, it has been experimentally observed that ethanol molecules adsorb on the TiO_xC_y surface, inhibiting its oxidation. This result has been confirmed by using *in situ* Fourier transform infrared spectroscopy (FTIRS). The adsorption of ethanol is expected to favour the EOR in the presence of suitable catalyst nanoparticles supported on TiO_xC_y.

Introduction

Direct Ethanol Fuel Cells (DEFCs) are very promising alternative energy conversion systems, having the advantages of easier handling, storage and transport of the fuel than gaseous hydrogen.[1]

The main advantage of using ethanol as fuel is that it can be obtained as bioethanol from agricultural products. Nowadays, the catalysts used for ethanol electrooxidation are based on Pt or Pt-alloy nanoparticles, mainly Pt-Sn alloys, supported on carbon materials.[2,3] Using these catalysts, high yields of partial oxidation products, CH_3CHO and CH_3COOH, are obtained, releasing two and four electrons per ethanol molecule, hence generating low energy conversion efficiency. In order to reach complete oxidation of ethanol to CO_2, releasing twelve electrons per molecule and generating higher energy conversion efficiency, higher operating temperatures (often referenced as intermediate-T, 150 – 200 °C) and appropriate catalysts are required to break the C-C bond.

It is known that one of the major contributors to catalyst failure in fuel cells (FCs) is the corrosion of the carbon materials used as electrocatalyst support. Under operating conditions, the oxidation of the carbon support occurs, leading to agglomeration of the catalyst nanoparticles and, therefore, to a loss of FC performance. If the operating temperature of the FC is increased, the carbon corrosion will be even more significant. Therefore, alternative support materials need to be investigated to fulfil the FC durability requirements at intermediate-T.

Early transition metal (groups IV – VI) carbides have recently attracted much interest due to their possible use in electrocatalysis,[4,5,6] both as catalysts[7,8] and supports.[6,9,10,11,12,13] Since they show similar electronic and catalytic properties as the Pt-group metals and present high conductivity and CO tolerance, they are potential substitutes for Pt as electrode materials for

FCs.[14] For this reason, they have been studied as electrocatalysts and electrocatalyst supports in different reactions, such as the oxidation of hydrogen, CO,[15,16] alcohol[12,17] and water,[18,19] as well as in the oxygen reduction reaction (ORR).[18,19] Recently, early transition metal carbides have also been tested as support materials due to their electrochemical (EC) stability to corrosion,[20] in order to replace standard carbon materials,[12,13,21] especially for intermediate-T applications. One major issue regarding their use as support material is associated with their stability under EC conditions. In fact, their transformation into corresponding oxides and/or oxycarbides can occur when operating in air and in solution.[20,22,23] Molybdenum[15,24] and tungsten[14,25] carbides have been the most studied materials, although titanium carbide has gained importance in the last few years.[13] In a previous work,[26] we already studied the Pt/TiO_xC_y planar system (Pt deposited on TiO_xC_y film) for the EOR up to 80 °C, obtaining higher activity and stability than with Pt on a glassy carbon (GC) electrode. In the literature, it has been reported that the addition of oxygen to TiC can be of great importance due to its high reactivity with most of the metals and the possibility of tailoring the optical and mechanical properties between those of metallic-like carbides and the ones of the corresponding oxides just by varying the oxygen/carbon ratio.[27] Therefore, early transition metal oxycarbides can be an obvious choice for tailoring alternative substrates to carbon for high temperature FCs.

In a previous paper, we reported a detailed surface science and theoretical study on the conversion of anodic TiO_2 films into TiO_xC_y in ultra-high-vacuum (UHV).[28] The intrinsic stability of the TiO_xC_y in UHV was discussed in detail and important information was obtained on the nature of the TiO_xC_y surface under ambient conditions: the *real* surface of a TiO_xC_y film consists of a nanocomposite where TiO_xC_y, TiO_2 and carbon are present.

Since an electrocatalyst support must be stable under reaction conditions, it is necessary to study its behavior under operating EC conditions. For this reason, in this work we have investigated the behavior of the mentioned TiO_xC_y planar system under EC conditions in order to get a clear description of the chemical changes of TiO_xC_y induced by electrochemical polarization of the material. To this end, we used a custom-built EC flow microcell connected to the UHV chamber by a transfer system under controlled atmosphere. This set-up allows us to couple EC with photoemission measurements, which furnish a detailed follow-up of the electrochemically induced transformations, avoiding the ambient effects. We have also used the density functional theory (DFT) approach to describe the phenomena occurring at the electrode interface under electrochemical conditions (theoretical Pourbaix diagrams), adopting a simplified surface model of the TiO_xC_y system. Furthermore, we have prepared TiO_xC_y powders and carried out spectroelectrochemical studies by *in situ* FTIRS at 25 °C and EC experiments under low pressure at 25 °C and 150 °C in order to determine the EC stability of this material and its suitability as electrocatalyst support for intermediate-T DEFCs.

Experimental

Combined chemical and electrochemical characterization of planar systems.

The chemical and electrochemical characterization of the TiO_xC_y planar system was conducted in a UHV-EC transfer system described in the SI. The chemical composition and chemical changes induced by the electrochemical work were determined by X-ray photoelectron spectroscopy (XPS). Photoemission data was obtained in a custom designed UHV system equipped with a EA 125 Omicrom electron analyzer equipped with five chaneltrons, working at a base pressure of 10^{-9} mbar. Core level photoemission spectra (C 1*s*, Ti 2*p* and O 1*s* regions)

were collected at room temperature with a non-monochromatized Mg K_α X-ray source (1253.6 eV) and using 0.1 eV steps, 0.5 s collection time and 20 eV pass energy. Measurements were performed both in normal emission and at grazing angle in order to increase the bulk and surface sensitivity, respectively.

A custom made PEEK (polyether ether ketone) cell was used for the electrochemical measurements. A Pt wire was used as counter electrode and an $Ag/AgCl/Cl^-_{(3M\ KCl)}$ electrode placed in a Luggin capillary was used as reference electrode. All the potentials in the text are referred to the reversible hydrogen electrode (RHE). The cell was controlled by an Autolab potentiostat running with NOVA 1.8 Software. The EC experiments were carried out both in deaerated 0.5 M H_2SO_4 and 0.5 M CH_3CH_2OH + 0.5 M H_2SO_4 solutions, prepared from high purity reagents (Sigma-Aldrich). The electrolyte was pumped into the EC cell through a tubing system using a syringe pump (N-1010, Pump Systems Inc.), which allows an accurate control of the flow. The electrolyte inlet consists of a capillary tube (diameter ca. 0.35 mm) placed in the centre of the cell, whereas the outlet is constituted by eight holes (diameter 0.5 mm) placed around the central capillary. Prior to the EC measurements, the tubing system was cleaned with Ar in order to remove the oxygen and then, it was filled with the electrolyte. All the electrochemical experiments were carried out at room temperature, in Ar atmosphere in order to avoid the contact of the sample with oxygen, and using a flow rate of 1 mL min^{-1}.

First, the sample was characterized by cyclic voltammetry (CV) in order to determine the main oxidation/reduction processes. With this aim, it was cycled between 0 V and 0.5 V and, subsequently, between 0 V and 1.1 V using a scan rate of 0.020 V s^{-1} until the voltammogram was stable (20 cycles). In second place, in order to confirm the EC oxidation/reduction processes

that take place on the surface of the TiO_xC_y film, chronoamperometric curves were recorded at different potentials for 1500 s.

Electrochemical characterization of powders.

Room temperature measurements. Cyclic voltammetry was used to determine the electrochemical behaviour of the TiO_xC_y material in absence and presence of 0.5 M ethanol (EtOH, Merck p.a.). Electrochemical measurements were carried out in a standard three-electrode electrochemical cell with an Autolab PGSTAT302 (Ecochemie) potentiostat. The working electrode consists of 20 μL of catalyst ink (4 mg ml^{-1} of catalyst) deposited onto a glassy carbon electrode of 7 mm in diameter. A carbon rod was used as counter electrode and a reversible hydrogen electrode (RHE) in the supporting electrolyte was employed as reference electrode. All potentials in the text are referred to this electrode. All solutions were prepared using ultrapure water (Millipore Milli-Q system).

Intermediate temperature (150 °C) measurements. CVs at high temperature were acquired in a pressure vessel equipped with three electrical connections suitable for running three electrode electrochemical cell experiments. The body of the pressure vessel is stainless steel. In order to avoid contaminations, the inner part was filled with a PTFE liner. The head of the vessel was also coated with PTFE in order to avoid steel corrosion provoked by the vapor condensation. Experiments were performed at 150 °C with the electrolyte in equilibrium with its vapor. The pressure under working conditions was between 5 and 6 atm depending on the electrolyte composition. The reference electrode was $Ag/AgCl/Cl^-_{(1M\ KCl)}$. We used this electrode for the high stability of Ag/AgCl electrode in harsh environment. Indeed, high pressure and high temperature uses have been previously reported, especially in nuclear industry where they have

been applied to monitor steel corrosion at temperatures exceeding 200 °C. To quote the potential *vs*. the RHE scale, we first converted Ag/AgCl values to the SHE scale according to the value reported by Greely[29] and, subsequently, we applied the correction between the SHE and RHE scale according to its temperature dependence: $E = \frac{RT}{F} pH$, where R is the universal gas constant, T the absolute temperature, F the Faraday constant and pH the pH of the electrolyte solution. The working electrode was a glassy carbon disk (5 mm diameter, Pine rotating disk electrode) modified in house for high temperatures (the original one cannot go over 80 °C), and a carbon rod was used as counter electrode. The inks were deposited on the glassy carbon electrode surface with the same procedure used for low temperature measurements. During the heating time, the working electrode potential was kept between 0.10 and 0.20 V *vs*. RHE. This interval comes from the fact that temperature changes while heating the system and the RHE scale does it accordingly. The time taken to reach a stationary temperature at 150 °C was between 30 and 45 min.

In situ FTIR characterization.

In-situ Fourier transform infrared spectroscopy (FTIRS) experiments were performed with a Bruker Vector 22 spectrometer equipped with a mercury cadmium telluride detector. A small glass flow cell with a 60º CaF_2 prism at its bottom was used. The cell and experimental arrangements have been described in detail elsewhere.[30] Briefly, the working electrode consisted of 20 μL of the catalyst ink deposited as a thin layer over a polycrystalline gold disk (geometric area = 0.785 cm^2). Experiences involve the introduction of the working electrode in the working solution (0.5 M H_2SO_4 or 1 M CH_3CH_2OH + 0.5 M H_2SO_4) at a fix potential of 0.05 V. Then, FTIR spectra were acquired by averaging of 128 scans at 8 cm^{-1} resolution at selected potentials,

varying the potential from 0.05 V with a 0.05 V step in the positive going direction. The reflectance ratio R/R_0 was calculated, where R and R_0 are the reflectances measured at the sample and the reference potential, respectively. In this way, positive and negative bands represent the loss and gain of species at the sampling potential, respectively.

Results and discussion

Electrochemical behavior of the TiO_xC_y planar system.

The TiO_xC_y substrate was prepared by carbothermal treatment of an anodic TiO_2 film (53 nm average thickness, obtained from anodization of polycrystalline Ti) in ethylene atmosphere ($5x10^{-6}$ mbar) at 550 °C in ultra-high vacuum (UHV) as described in ref. [28]. Subsequently, it was analyzed by XPS to determine the chemical composition. The spectra were acquired at different angles in order to study the in-depth homogeneity of the film. As already seen in our previous work,[28] the films obtained under these conditions are very uniform with a slight enrichment of graphitic carbon (peak at 284.5 eV in the C 1*s* photoemission line) and TiO_x species (component at 456.8-457.4 eV in the Ti 2*p* photoemission line and component at 530.2 eV in the O 1*s* photoemission line) on the surface (see spectra acquired at θ = 30° in Figure S1, which are more sensitive to the surface). The films prepared under these conditions had a $TiO_{0.5}C_{0.5}$ stoichiometry and contain a small amount of fully converted TiC.

After the synthesis and chemical characterization, the sample was transferred to the EC cell. The sample was first characterized by CV in order to determine the main oxidation/reduction processes. With this aim, 20 CVs were recorded between 0.0 V and 0.5 V and, subsequently, another 20 CVs were acquired between 0.0 V and 1.1 V. After the 20^{th} CVs, the current-potential profile was stable in both potential windows studied. After each EC measurement, the sample

was transferred back to the main chamber and the chemical changes caused by the EC work were determined by XPS. The results for both the EC and XPS measurements are reported in Figure 1.

During the first anodic sweep (red curve in Figure 1a), an anodic peak was observed at around 0.27 V, which could be attributed to the oxidation of Ti^{3+} (titanium suboxides seen by XPS), present on the surface of the film, to Ti^{4+} (TiO_2).[31] During the backward scan, the cathodic currents obtained at more negative potentials than 0.2 V could be associated to the formation of lower valence states such as Ti^{3+} from the TiO_2 thin film formed on the surface. In the literature, this cathodic current has been explained either as the formation of Ti^{3+} or the formation of titanium hydroxide on the outermost layer of the oxide film.[32,33] At potentials higher than 0.35 V, the anodic currents observed could be assigned to the oxidation of the TiO_xC_y component (residing below the outermost surface) to TiO_2. However, it is not possible to determine the onset potential for this process due to the overlap with the oxidation of the surface TiO_x species.

It should be noticed that, after the first cycle, the anodic current is almost negligible, suggesting that the oxidation of the film took place mainly during the first anodic sweep. The oxide film formed on the surface is stable and passivates the surface avoiding further oxidation of the underlying TiO_xC_y film. XPS analysis of the sample supports the partial oxidation of the film surface during the cycling treatment up to 0.5 V, which is evidenced by the appearance of a new component at 459 eV in the Ti 2*p* photoemission line, associated to TiO_2. From the comparison of the Ti 2*p* region before and after the EC treatment up to 0.5 V (see also Table S1), it is confirmed that the TiO_2 formed comes from the oxidation of TiO_xC_y to TiO_x, and its further oxidation to TiO_2. The TiC present in the sample seems to be stable under these conditions. In addition, the hydration of the TiO_2 formed on the surface was detected (component at 460.2 eV in the Ti 2*p* line).

When the potential sweep is extended up to 1.1 V (Figure 1b, red line), the peak at 0.27 V is observed again, whereas the anodic current observed at potentials higher than 0.35 V is again associated with the oxidation of the TiO_xC_y component and growth of the TiO_2 thin film, in good agreement with the XPS results. However, in the currents obtained between 0.4 and 1.1 V, at least two different processes can be distinguished. The first one with a maximum current at around 0.6 V and the second one around 0.85 V. In the literature, it has been reported that TiC starts oxidizing at around 0.75 V,[16,34,35] therefore, we can associate the process at 0.85 V to the oxidation of the fully converted TiC (deduced from the decrease of the component at 454.5 eV in the Ti 2*p* PE) through the following reactions:

$$TiC + 3\ H_2O \rightarrow TiO_{2(s)} + 6\ H^+ + CO_{(g)} + 6\ e^- \quad (1)$$

$$TiC + 4\ H_2O \rightarrow TiO_{2(s)} + 8\ H^+ + CO_{2(g)} + 8\ e^- \quad (2)$$

The first process at 0.6 V could be associated with the oxidation of TiO_xC_y (deduced from the decrease of the component at 455.0 eV in the Ti 2*p* PE) leading to the formation of a TiO_2 film and CO and CO_2 species through the reactions (assuming that the film stoichiometry is $TiO_{0.5}C_{0.5}$):

$$2\ TiO_{0.5}C_{0.5} + 4\ H_2O \rightarrow 2\ TiO_{2(s)} + 8\ H^+ + CO_{(g)} + 8\ e^- \quad (3)$$

$$2\ TiO_{0.5}C_{0.5} + 5\ H_2O \rightarrow 2\ TiO_{2(s)} + 10\ H^+ + CO_{2(g)} + 10\ e^- \quad (4)$$

As a result of the oxidation of TiC and TiO_xC_y, an increase of the components related to TiO_2 (459.0 eV) and its hydration (460.2 eV) were observed in the Ti 2*p* PE.

It is important to be noted that the TiO_xC_y film remains underneath the TiO_2 thin film (see component at 455 eV in the Ti 2*p* photoemission line in Figure 1), and that the TiO_2 film is stable and protects the TiO_xC_y film from further oxidation at a given potential. This behaviour is

typical for the oxide growth described by the point defect model,[33,36] where the thickness of the film increases with the applied anodic potential.

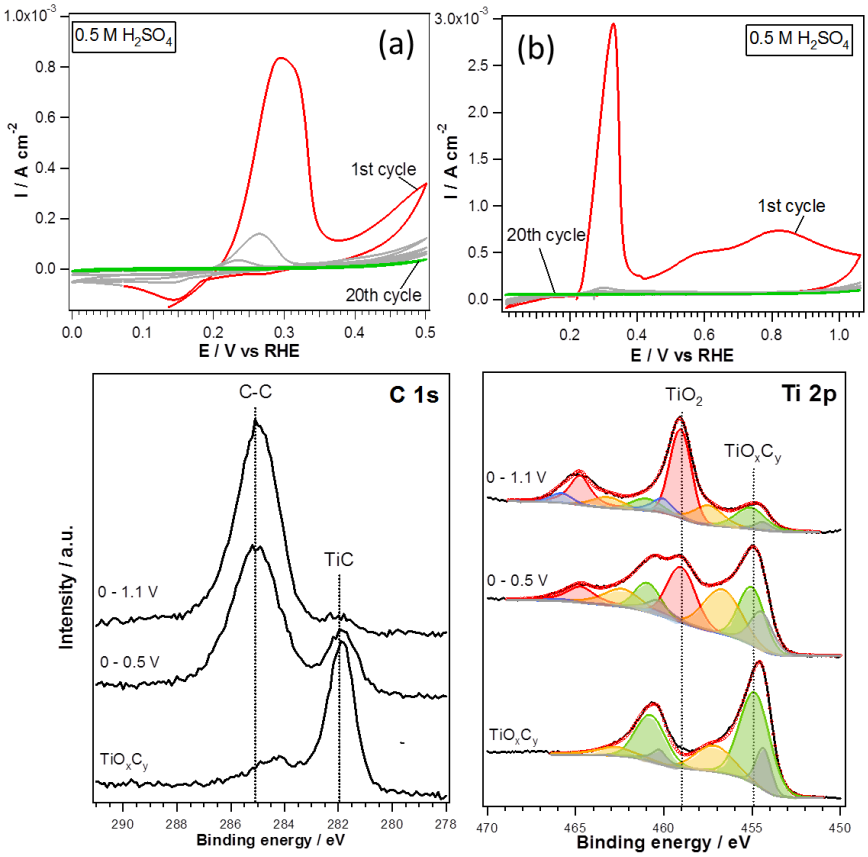

Figure 1. Upper panels: CVs between 0.0 V and 0.5 V (a, c) and 0.0 V and 1.1 V vs RHE (b, d) on the TiO_xC_y film in Ar-saturated 0.5 M H_2SO_4 at room temperature using a scan rate of 0.020 V s^{-1} and a flow rate of 1 mL min^{-1}. Bottom panels: Corresponding C 1*s* and Ti 2*p* XPS spectra (taken in normal emission), as well as the deconvolution of the Ti 2p region into single chemical components, for the TiO_xC_y film before and after the EC treatments. Assignment of components in Ti 2*p* region: TiC (grey), TiO_xC_y (green), TiO_x (yellow), TiO_2 (red) and $TiO_2 \cdot xH_2O$ (blue). The corresponding analysis of the fit can be found in Table S1.

In order to confirm the electrochemical oxidation/reduction processes that take place on the surface of the TiO_xC_y film, once they were identified by cyclic voltammetry, chronoamperometric curves were recorded at different potentials. The *i-t* curves and the corresponding XPS data are depicted in Figure 2. The potentials studied were: (i) 0 V, where the reduction of TiO_2 species at the surface is expected; (ii) 0.27 V, where the oxidation of Ti^{3+} to Ti^{4+} can take place; and (iii) 0.6 V where the oxidation of TiO_xC_y to TiO_2 is favoured. At 0 V, a small negative current was obtained. This cathodic current could be associated with the reduction of TiO_2, as explained above. The very low current could be explained by the almost negligible amount of TiO_2 on the as prepared sample surface. The Ti 2*p* PE line obtained at this potential did not show a significant change in the sample, compared with the one for the as prepared material. Only a slight decrease of the TiO_x species was observed (see Table S2), in agreement with the very small cathodic currents observed during the electrochemical measurement. The reduction of the TiO_x species was more evident from the O 1*s* PE line, where a decrease of the component at lower binding energies (corresponding to TiO_x species with $1 < x \leq 2$) was observed. At 0.27 V, however, anodic currents were observed. In fact, a small shoulder at 459 eV, associated with TiO_2, was observed in the Ti 2*p* photoemission peak. Taking the XPS data into account, the anodic current can be related to the oxidation of TiO_x to TiO_2,[31] but also to the slight oxidation of TiO_xC_y to TiO_x, since a decrease of the TiO_xC_y/TiC ratio is observed. In agreement with these changes in the Ti 2*p* line, an increase of the component at lower binding energies (530.2 3V) in the O 1*s* line takes place. At 0.6 V, however, significant oxidation of the surface occurred, leading to TiO_2 formation, evident from the growth of the components at 459 eV and 530.2 eV in the Ti 2*p* and O 1*s* PE lines, respectively. From the XPS data, it is deduced

that the oxidation currents observed at this potential come mainly from the oxidation of TiO_xC_y to TiO_x and its further oxidation to TiO_2.

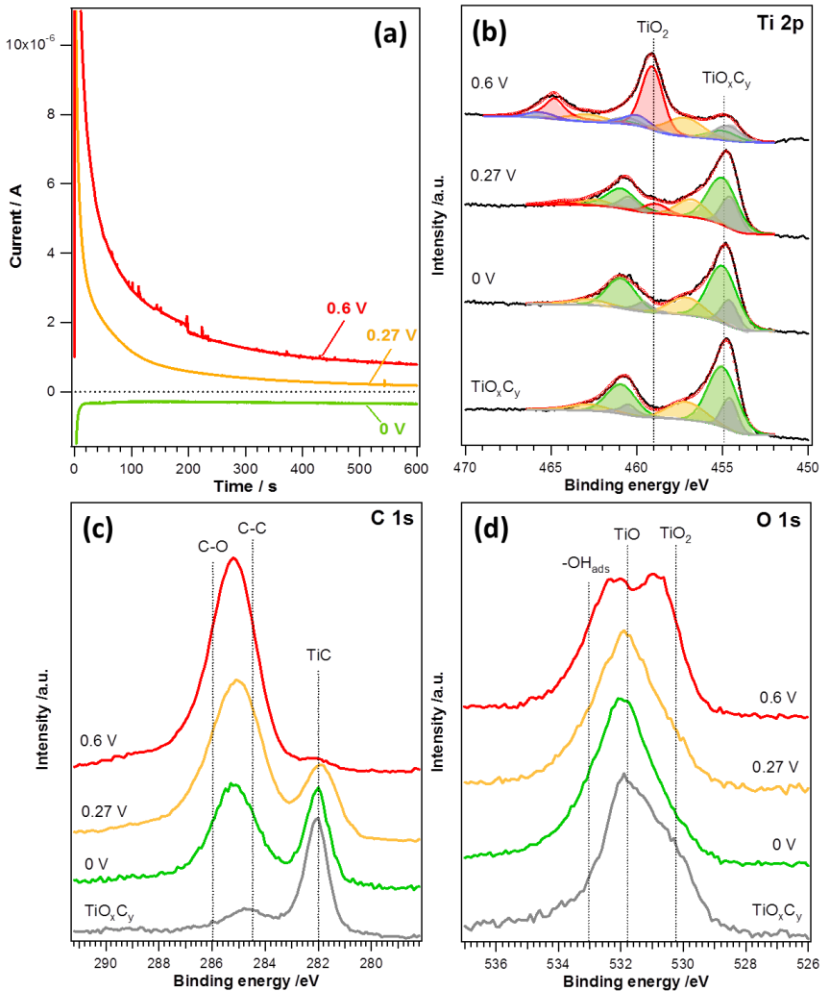

Figure 2. *i-t* curves obtained at different potentials (a); Ti 2*p*, as well as the separation into single chemical components (b); C 1*s* (c); and O 1*s* (d) PE lines (taken in normal emission) for the TiO_xC_y film before and after the EC measurements. The *i-t* curves were obtained in Ar-saturated 0.5 M H_2SO_4 using a flow rate of 1 mL min^{-1} and only an enlargement of the first 600 s is showed for clarity. Assignment of components in Ti 2*p* region: TiC (grey), TiO_xC_y (green), TiO_x (yellow), TiO_2 (red) and $TiO_2 \cdot xH_2O$ (blue). The corresponding analysis of the fit can be found in Table S2.

Since TiO_xC_y is currently studied to replace standard carbon supports in DEFCs operated at intermediate-T, the behavior of the material was also examined by cyclic voltammetry in presence of ethanol. The results are depicted in Figure 3. In this case, the peaks at 0.27 V and 0.15 V, related to the oxidation/reduction of TiO_x species present on the surface of the film, were not observed. The absence of these peaks could be explained by the preferential adsorption of ethanol on oxygen vacancies (i.e. TiO_x sites),[37] blocking their redox processes. However, the oxidation currents at higher potentials, associated with the TiO_xC_y oxidation, were still observed and they presented similar current profiles to those obtained in the supporting electrolyte but with lower intensities. Due to the absence of the oxidation peak at *ca*. 0.3 V, it is easier to determine the onset potential for the oxidation of TiO_xC_y, which is around 0.27 V.

The comparison of the Ti 2*p* spectra in absence and presence of ethanol confirms that the degree of oxidation was lower when ethanol was added to the electrolyte, since the TiO_xC_y/TiO_2 ratio is higher in presence of ethanol (see Table S1). As explained above, this fact can be attributed to the adsorption of ethanol, mainly on the TiO_x species but also on TiO_xC_y, inhibiting its oxidation, as seen in the CVs. It is also remarkable that, in presence of ethanol, the hydration of the TiO_2 film does not occur, which could be also related to the adsorption of ethanol. Regarding the C 1*s* photoemission line, the increase of the peak at 285 eV, both in the supporting electrolyte and in presence of ethanol, indicates that a layer of amorphous carbon is deposited on the surface of the film. This carbon layer comes mainly from the contamination of the electrolyte. The comparison of the C 1*s* spectra after the electrochemical treatments in sulphuric acid and ethanol electrolytes shows that the peak at 285 eV is broader at higher BEs when the

sample is exposed to ethanol. The new component at higher BE could be associated with ethanol adsorbed on the surface.

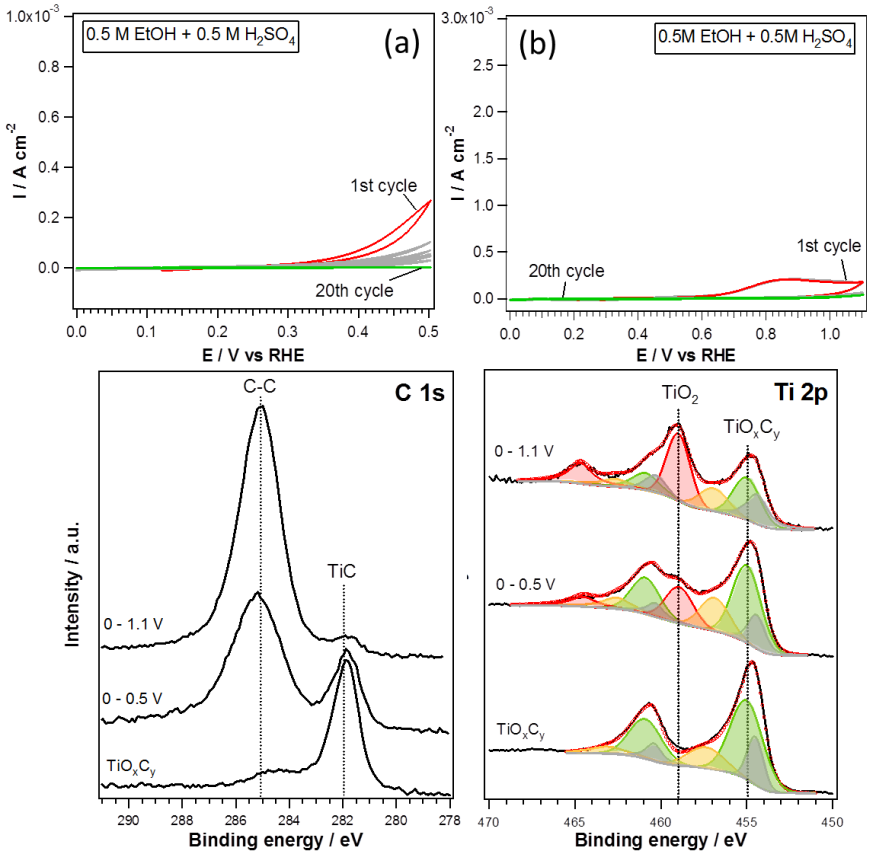

Figure 3. Upper panels: CVs between 0.0 V and 0.5 V (a, c) and 0.0 V and 1.1 V vs RHE (b, d) on the TiO_xC_y film in Ar-saturated 0.5 M CH_3CH_2OH + 0.5 M H_2SO_4 at room temperature using a scan rate of 0.020 V s^{-1} and a flow rate of 1 mL min^{-1}. Bottom panels: Corresponding C 1*s* and Ti 2*p* XPS spectra (taken in normal emission), as well as the deconvolution of the Ti 2*p* region into single chemical components, for the TiO_xC_y film before and after the EC treatments. Assignment of components in Ti 2*p* region: TiC (grey), TiO_xC_y (green), TiO_x (yellow) and TiO_2 (red). The corresponding analysis of the fit can be found in Table S1.

DFT studies of a $TiO_{0.5}C_{0.5}$ model system.

In order to get more insight into the phenomena occurring at the material surface under electrochemical condition, we have adopted DFT and the computational standard hydrogen electrode formalism[38] extensively used in the literature. The details of the procedure and model used for the calculations are described in the SI. This allowed computing theoretical Pourbaix diagrams and predicting the overpotential for e.g., for the oxygen evolution reaction (OER):

$$H_2O_{(l)} \rightarrow \frac{1}{2} O_{2(g)} + 2H^+ + 2e^- \quad (5)$$

Modelling anodization processes is by far more complex than modelling the OER, because of the strong structural and stoichiometry changes undergone by the electrode surface. It is however likely that the early stages of anodization involve the same elementary processes of the OER, i.e. those described in Equations 1 and 2 in the SI. Even this limited task represents a challenge, as no detailed information about the actual distribution of the atoms of the constituent elements is available, neither in the bulk nor at the surface. Because the number of possible structures is very large, we reduced them taking into consideration a prototypical system, already studied in Ref. 28, where O and C atoms are present in an equal quantity and are perfectly mixed. This system has the advantage that its surface can be described using a small rectangular unit cell, sketched in Figure S2. Four different species are exposed at the surface, as the two Ti atoms, indicated as Ti1 and Ti2, are not equivalent (they stay on top of an O and of a C atom, respectively, see Figure S2). We considered a six layer centrosymmetric model, where adsorbates are placed at both surfaces.

When the surface is exposed to an aqueous environment, species present therein can be adsorbed on the exposed atoms. As various species (in the first place H*, OH* and O*, where * indicates a surface site, and *X** indicates an adsorbed *X* species) can be adsorbed at four inequivalent sites, it turns out that even our simplified model requires dealing with several

possible configurations. In order to limit the number of investigated configurations, we first determined the preferred site for each species, comparing the total energies of the adsorption complexes for all the sites. It turns out that H* prefers the C site, whereas OH* and O* prefer the Ti1 site (see Table S3). Most notably, OH* has not even a local minimum at the C site, whereas O* prefers the Ti1 and Ti2 sites over the C one by 1.60 and 0.54 eV, respectively. This means that, though the anodization process involves the oxidation of lattice C atoms to CO_2 (see above), the process is not likely to be started by a direct attack to C sites. Furthermore, the O* species, which has a very strong preference for the Ti1 site, gives rise to a strong rearrangement of the surface, where the Ti1 ions are displaced by half a lattice constant along the ***b*** direction, forming a chain of tetrahedrally coordinated species (see Figure 4a).

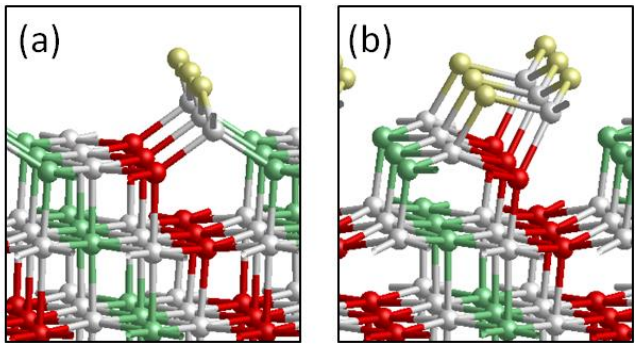

Figure 4. Sketches of the equilibrium configurations corresponding to: (a) One O* species adsorbed at the Ti1 site. (b) Two O* species adsorbed to the Ti1 and Ti2 sites. O* atoms are depicted as gold spheres. Ti, O and C atoms are represented as grey, red and green spheres.

We next examine what happens when a further adsorbate is placed on the surface. This is done by adding one adsorbate among the H*, OH* and O* species on one of the unoccupied sites while keeping the first adsorbate on its preferred site. Free energies of formation at 298 K for all the possible configurations were computed and plotted as a function of the potential at pH = 0 in

Figure S3. It turns out that, between -0.4 V and 1.1 V, the stable configuration is obtained by placing a OH* species on the Ti2 site of the configuration shown in Figure 4a. At higher potentials, the surface is further oxidized, and gives rise to the configuration shown in Figure 4b. The O* adsorbate, initially placed as a terminal ion on top of Ti2, spontaneously forms a bridge to the Ti1 ion, which in turn detaches from the C atom to which it was bonded. On one hand, this gives rise to a TiO_x polymer whose structure contains some of the structural motifs of the TiO_2 anatase polymorph. On the other hand, surface C atoms are left exposed and suitable to be oxidized to CO_2 as experimentally observed (see FTIR results below).

Summarizing, DFT calculations show that there are two non equivalent Ti sites (Ti1 and Ti2, on top of an O and of a C atom, respectively) and that the oxidation process starts from the Ti1 site, producing TiO_2-like structures. These transformations leave the surface C atoms undercoordinated and exposed to further attacks.

Electrochemical behavior of the TiO_xC_y powders.

High-surface area TiO_xC_y powder was obtained using methylcellulose (MC) as carbon source and titanium diethanolamine as Ti precursor. The synthesis process is described in detail in the SI. The TiO_xC_y powder showed a sponge-like morphology (see Figure S4a) with a high specific surface area of 257 $m^2\ g^{-1}$ and a bimodal pore size distribution, with average pore diameters of 1 nm and 4 nm. The stoichiometry was obtained from the XRD analysis and resulted to be $TiO_{0.49}C_{0.51}$ with absence of titanium suboxides (see Figure S4b). Synthetized TiO_xC_y powders presented fast electron transfer (with a conductivity similar to GC), which is measured using cyclic voltammetry in the presence of a $[Fe(CN)_6]^{3-/4-}$ redox couple, where a peak separation of 60 mV between the anodic and cathodic peaks is found (Figure S5).

The TiO_xC_y powder was electrochemically characterized and compared to the TiO_xC_y films studied above. Figures 5a and 5b show the CVs recorded at room temperature in 0.5 M H_2SO_4 and 1 M CH_3CH_2OH + 0.5 M H_2SO_4 solutions, respectively. The electrochemical response of TiO_xC_y powder in 0.5 M sulphuric acid solution shows an irreversible anodic peak at *ca*. 1.1 V with an onset potential of around 0.9 V (Figure 5a). The onset potential for the oxidation of the TiO_xC_y powder is attained at higher potentials than those for the TiO_xC_y film. This is due to the already oxidized surface of the powder due to contact with air. It is remarkable that, in the subsequent cycles, the anodic contribution falls. This suggests irreversible oxidation during the first anodic sweep, producing a stable surface, in agreement with that observed at planar TiO_xC_y electrodes. Figure 5b shows analogous potentiodynamic experiments carried out in the presence of ethanol, in which similar results to those obtained on planar TiO_xC_y films are achieved, *i.e*. the anodic currents at higher potentials than 0.9 V are inhibited presumably by adsorbed ethanol residues.

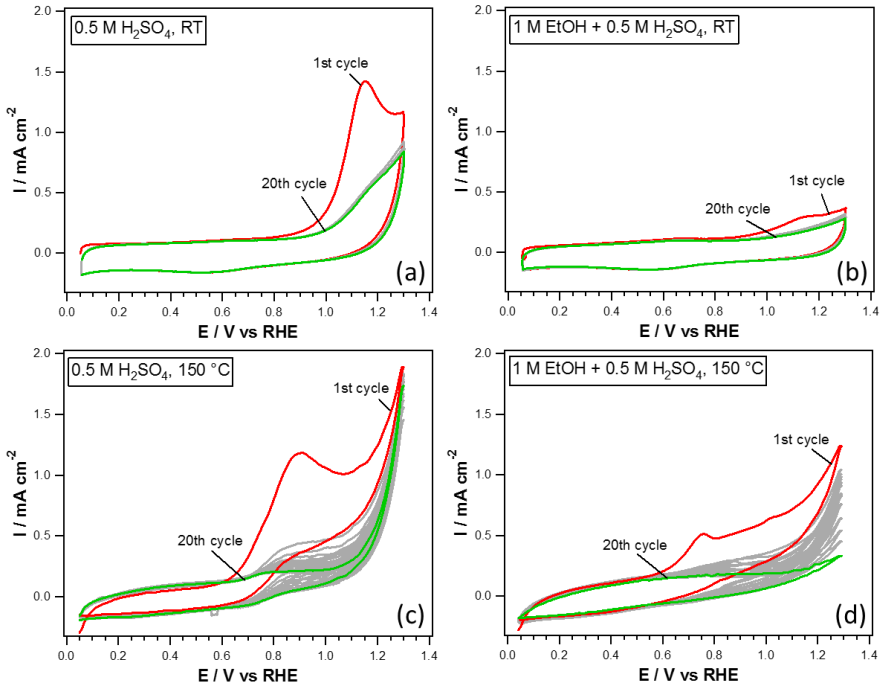

Figure 5. CVs between 0.05 V and 1.3 V vs RHE at the TiO_xC_y powder in Ar-saturated 0.5 M H_2SO_4 (a, c) and 0.5 M CH_3CH_2OH + 0.5 M H_2SO_4 (b, d) solutions at room temperature (a, b) and 150 °C (c, d) using a scan rate of 0.020 V s^{-1}.

To understand the electrochemical reactions associated with the anodic currents developed on TiO_xC_y powder in absence and presence of ethanol, *in situ* FTIRS was employed. Spectra were recorded by applying single potential steps from a reference potential (0.05 V) in the positive-going direction. In the spectra, negative and positive bands are related to the formation and consumption of species, respectively. Figure 6a shows the spectra recorded in sulphuric acid solution, where only the signal at 2343 cm^{-1}, associated to CO_2 formation, is discerned at potentials higher than 0.8 V. Therefore, the anodic faradaic current developed on TiO_xC_y powder at higher potentials than 0.8 V is associated with material corrosion, *i.e*. oxygenated species formation.

It is remarkable that the results obtained for TiO_xC_y powder are close to those obtained for planar TiO_xC_y systems and DFT calculations, therefore, confirming that reaction 4 occurs at the powder electrode. Nevertheless, unless CO was not detected, reaction 3 cannot be discarded since previous works observed the formation of carbon monoxide on TiC surface in sulphuric acid solution by FTIRS.[16,19] It is remarkable that the results obtained for TiO_xC_y powder are close to those obtained for planar TiO_xC_y systems and DFT calculations, therefore, reactions 3 and 4 may happen at the powder electrode. Thus, the oxide film formed on the surface of the powder is not reduced during the backward scan and it is insoluble in the electrolyte (with the exception of CO_2), as can be deduced by the absence of the anodic peak during the subsequent scans. As described above, this behaviour suggests surface oxidation, which avoids further corrosion and maintains high conductivity (Figure S5). Figure 6b shows analogous infrared

experiments but performed in presence of ethanol. As observed in Figure 6b, only the band associated to CO_2 (2343 cm^{-1}) is observed. The main difference between the experiments in absence and presence of ethanol is the onset potential for the CO_2 formation, which is shifted 0.2 V to more positive potentials in presence of the dissolved alcohol. In addition, the infrared band intensities attributed to CO_2 formation are smaller in presence of the alcohol in solution. These results agree with the observations reported for planar TiO_xC_y, in which a smaller amount of TiO_2 was observed by XPS analysis in presence of ethanol. Therefore, adsorbed ethanol residues seem to inhibit the water dissociation on the TiO_xC_y surface and, consequently, the surface oxidation of the TiO_xC_y material. This result is of paramount importance since ethanol adsorption is the first step for the ethanol oxidation reaction.

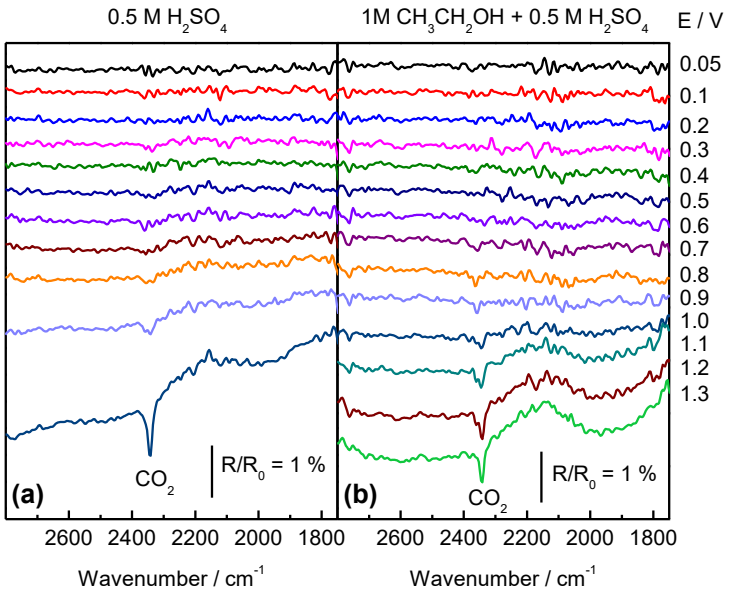

Figure 6. *In situ* FTIR spectra taken at different potentials in 0.5 M H_2SO_4 (a) and 1 M CH_3CH_2OH + 0.1 M H_2SO_4 (b) at the TiO_xC_y powder.

The investigation of the electrochemical behavior of the TiO_xC_y powder has been extended to intermediate-T range (i.e. 150 °C), in order to determine the suitability of this material as

electrocatalyst support for intermediate-T DEFCs. Figures 5c and 5d show the response of the TiO_xC_y powder at 150 °C in 0.5 M H_2SO_4 and 0.5 M H_2SO_4 + 1 M CH_3CH_2OH, respectively. At room temperature, high oxidation currents, attributed to the surface oxidation of TiO_xC_y to TiO_2, are observed in the first anodic sweep. In this case, a shift of the onset potential towards more negatives potentials (around 0.6 V), compared with that at RT, is produced due to the effect of the temperature. In agreement to the observations at RT, an anodic current drop occurred during the following cycles, indicating that the irreversibility of the oxidation is preserved at 150 °C. In presence of ethanol, the CV profile is the same as that obtained in the supporting electrolyte; however, the anodic peak current density is lower in presence of the alcohol at the same temperature. At 150 °C this effect is not as dramatic as at 25 °C, where the suppression of the anodic peak was much more evident (Figures 5a and 5b), which could be ascribed to the decrease of the adsorption coverage of ethanol related species provoked by the increase of the temperature.

Taking into account that DEFCs operate at *ca*. 0.5-0.6 V at working temperatures around 80 ºC, and that the working potential is expected to be lower at intermediate-T (150-200 ºC), it is predictable that TiO_xC_y material will be suitable under EOR conditions for a wide temperature range of operation (T < 200 ºC).

Conclusions

A detailed study of the electrochemical stability of TiO_xC_y under working EOR conditions, as well as of the chemical changes induced by the electrochemistry, was performed in order to determine the suitability of this material as substitute for carbon supports in intermediate-T DEFCs.

The oxidation of the TiO_xC_y substrate was studied combining photoemission and electrochemical measurements carried out on a TiO_xC_y planar system prepared in UHV conditions: the titanium suboxides (TiO_x) species present on the surface of the film start to oxidize at around 0.2 V forming TiO_2, whereas the underneath TiO_xC_y does at around 0.3 V. Two different processes have been identified for the TiO_xC_y oxidation, which can be associated to the presence of TiC and TiO_xC_y segregated phases. Their oxidation leads to the formation of TiO_2 and CO_2. This TiO_2 overlayer is stable and prevents full oxidation of the TiO_xC_y sample, leading to a stable electrode material at the EOR working conditions (0.3 – 0.6 V). In presence of ethanol, ethanol molecules adsorb on the surface (preferentially at TiO_x species) preventing further oxidation of the material.

The electrochemical study performed on TiO_xC_y powders at room temperature and 150 °C led to the same conclusions. The only difference between the powders and the planar system is that the onset potential for the oxidation of TiO_xC_y is shifted to higher potentials in the case of the powders due to the presence of TiO_2 on the surface, formed due to the previous exposure to air. Ethanol adsorption was also observed on the powders at low and high temperatures. The inhibition of the TiO_xC_y oxidation due to the adsorption of ethanol residues was confirmed by *in situ* FTIRS measurements, in which a lower amount of CO_2 was produced in presence of the alcohol.

Therefore, this study demonstrates that TiO_xC_y is a suitable alternative to carbon based supports for intermediate-T DEFCs due to its electrochemical stability and conductivity under EOR conditions and, in addition, it is expected that the adsorption of ethanol on TiO_xC_y will favour its subsequent oxidation on the supported catalyst nanoparticles.

Supporting Information. The description of the UHV system used for the preparation and characterization of the planar system; the analysis of the deconvolution of the Ti 2*p* PE lines; the description of the model system and the details used for the DFT calculations; the synthesis and physicochemical characterization of the powders; and the electrodes preparation and the determination of the electron transfer resistance are presented. This material is available free of charge via the Internet at http://pubs.acs.org.

Corresponding Author

* gaetano.granozzi@unipd.it.

Present Addresses

§ Advanced Light Source, Lawrence Berkeley Laboratory, Berkeley, CA 94720, USA.

Author Contributions

The manuscript was written through contributions of all authors. The manuscript reports a part of the results of the EU project DECORE. LC and SA studied the planar systems; AP and AM synthesized and characterized the powders physicochemically; GGa and OGV performed the (*in situ*) electrochemistry of the powders; CVV and JKL determined the electron transfer resistance of the powders and supplied the anodic TiO_2 films; AV did the DFT calculations; MB and AL carried out the electrochemical measurements of the powders at high temperature; LC, GGa, EP, JKL and GGr drafted the manuscript and GGr coordinated the work. All authors have given approval to the final version of the manuscript.

ACKNOWLEDGMENT

The authors acknowledge the European Union Seventh Framework Programme support via the EU project DECORE (Project 0309741) under Contract No. FP7-NMP-2012- SMALL-6 for Research and Technological Development.

REFERENCES

(1) Lamy, C.; Lima, A.; LeRhun, V.; Delime, F.; Coutanceau, C.; Léger J.-M. Recent Advances in the Development of Direct Alcohol Fuel Cells (DAFC). *J. Power Sources*, **2002**, *105*, 283-296.

(2) Asgardi, J.; Calderón, J.C.; Alcaide, F.; Querejeta, A.; Calvillo, L.; Lazaro, M.J.; Garcia, G.; Pastor, E. Electrocatalysis of Ethanol Electrooxidation on Pt-Sn Supported Alloys. Comparison Between Ex Situ Kinetic Measurements and Direct Ethanol Fuel Cell Experiments. *Appl. Catal. B: Environ*. **2015**, *168-169*, 33-41.

(3) Jin, J.-M.; Sheng, T.; Lin, X.; Kavanagh, R.; Hamer, P.; Hu, P.; Hardacre, C.; Martinez-Bonastre, A.; Sharman, J.; Thompsett, D.; Lin, W.-F. The Origin of High Activity but Low CO_2 Selectivity on Binary PtSn in the Direct Ethanol Fuel Cell. *Phys. Chem. Chem. Phys*. **2014**, *16*, 9432-9440.

(4) Ham, D. J.; Lee, J. S. Transition Metal Carbides and Nitrides as Electrode materials for Low Temperature Fuel Cells. *Energies* **2009**, *2*, 873-899.

(5) Huang, K.; Li, Y.; Xing, Y. Carbothermal Synthesis of Titanium Oxycarbide as Electrocatalyst Support with High Oxygen Evolution Reaction Activity. *Mater. Res*. **2013**, *28*, 454-460.

(6) Rüdiger, C.; Maglia, F.; Leonardi, S.; Sachsenhauser, M.; Sharp, I. D.; Paschos, O.; Kunze, J. Surface Analytical Study of Carbothermally Reduced Titania Films for Electrocatalysis Application. *Electrochim. Acta* **2012**, *71*, 1-9.

(7) Christian, J.B.; Smith, S.P.E.; Whittingham, M.S.; Abruna, H.D. Tungsten Based Electrocatalyst for Fuel Cell Applications. *Electrochem. Commun*. **2007**, *9*, 2128-2132.

(8) Stottlemyer, A.L.; Weigert, E.C.; Chen, J.G. Tungsten Carbides as Alternative Electrocatalysts: From Surface Science Studies to Fuel Cell Evaluation. *Ind. Eng. Chem. Res*. **2011**, *50*, 16-22.

(9) Antolini, E.; Gonzalez, E.R. Ceramic Materials as Supports for Low-Temperature Fuel Cell Catalysts. *Solid State Ionics* **2009**, *180*, 746-763.

(10) Liu, Y.; Kelly, T. G.; Che, J. G.; Mustain, W. E. Metal Carbides as Alternative Electrocatalyst Supports. *ACS Catal*. **2013**, *3*, 1184-1194.

(11) Shao, Y.; Liu, J.; Wang, Y.; Lin, Y. Novel Catalyst Support Materials for PEM Fuel Cells: Current Status and Future Prospects. *J. Mater. Chem*. **2009**, *19*, 46-59.

(12) Roca-Ayats, M.; García, G.; Galante, J.L.; Peña, M.A.; Martínez, M.V. TiC, TiCN, and TiN Supported Pt Electrocatalysts for CO and Methanol Oxidation in Acidic and Alkaline Media. J. *Phys. Chem. C* **2013**, *117*, 20769-20777.

(13) Ou, Y.; Cui, X.; Zhang, X.; Jiang, Z. Titanium Carbide Nanoparticles Supported Pt Catalysts for Methanol Electrooxidation in Acidic Media. *J. Power Sources* **2010**, *195*, 1365-1369.

(14) Weigert, E.C.; Stottlemyer, A.L.; Zellner, M.B.; Chen, J.G. Tungsten Monocarbide as Potential Replacement of Platinum for Methanol Electrooxidation. *J. Phys. Chem. C*. **2007**, *111*, 14617-14620.

(15) R. Guil-Lopez, M.V. Martinez-Huerta, O. Guillen-Villafuerte, M.A. Peña, J.L.G. Fierro, E. Pastor, Highly dispersed molybdenum carbide as non-noble electrocatalyst for PEM fuel cells: Performance for CO electrooxidation, *Int. J. Hydrogen Energ*. **2010**, *35*, 7881-7888.

(16) Roca-Ayats, M.**;** García, G.**;** Peña, M. A.**;** Martínez-Huerta, M. V. Titanium Carbide and Carbonitride Electrocatalyst Supports: Modifying Pt–Ti Interface Properties by Electrochemical Potential Cycling. *J. Mater. Chem. A* 2014, *2*, 18786-18790.

(17) Macak, J.M.; Barczuk, P.J.; Tsuchiya, H.; Nowakowska, M.Z.; Ghicov, A.; Chojak, M.; Bauer, S.; Virtanen, S.; Kulesza, P.J.; Schmuki, P. Self-Organized Nanotubular TiO_2 Matrix as Support for Dispersed Pt/Ru Nanoparticles: Enhancement of the Electrocatalytic Oxidation of Methanol. *Electrochem. Commun*. **2005**, *7*, 1417-1422.

(18) García, G.; Roca-Ayats, M.; Lillo, A.; Galante, J.L.; Peña, M.A.; Martínez-Huerta, M.V. Catalyst Support Effects at the Oxygen Electrode of Unitized Regenerative Fuel Cells, *Catal. Today* **2013**, *210*, 67-74.

(19) Roca-Ayats, M.; García, G.; Galante, J.L.; Peña, M.A.; Martínez-Huerta, M.V. Electrocatalytic Stability of Ti Based-Supported Pt_3Ir Nanoparticles for Unitized Regenerative Fuel Cells, *Int. J. Hydrogen Energy* **2014**, *39*, 5477-5484.

(20) Kimmel, Y.C.; Xu, X.; Yu, W.; Yang, X.; Chen, J.G. Trends in Electrochemical Stability of Transition Metal Carbides and Their Potential Use as Supports for Low-Cost Electrocatalysts. *ACS Catal*. **2014**, *5*, 1558-1562.

(21) Wang, Y-J.; Wilkinson, D. P.; Zhang, Non carbon Support Materials for Polymer Electrolyte Membrane Fuel Cell Electrocatalysts. *J. Chem. Rev*. **2011**, *111*, 7625-7651.

(22) Zellner, M.B.; Chen, J.G. Surface Science and Electrochemical Studies of WC and W_2C PVD Films as Potential Electrocatalysts, *Catal. Today* **2005**, *99*, 299-307.

(23) Weidman, M.C.; Esposito, D.V.; Hsu, J.G. Chen, Y.-C. Comparison of Electrochemical Stability of Transition Metal Carbides (WC, W2C, Mo_2C) over a Wide pH Range. *J. Power Sources* **2012**, *202* 11-17.

(24) Guillen-Villafuerte, O.; Guil-Lopez, R.; Nieto, G. Garcia, E.; Rodriguez, J.L.; Pastor, E.; Fierro, J.L.G. Electrocatalytic Performance of Different Mo-Phases Obtained During the Preparation of Innovative Pt-MoC Catalysts for DMFC Anode. *Int. J. Hydrogen Energ*. **2012**, *37*, 7171-7179.

(25) Antolini, E.; Gonzalez, E. R. Tungsten-Based Materials for Fuel Cell Applications. *Appl. Catal. B: Environ*. **2010**, *96*, 245-266.

(26) Rüdiger, C.; Brumbarov, J.; Wiesinger, F.; Leonardi, S.; Paschos, O.; Valero-Vidal, C.; Kunze- Liebhäuser, J. Ethanol Oxidation on TiO_xC_y-Supported Pt Nanoparticles. *ChemCatChem* **2013**, *11*, 3219-3223.

(27) Fernandes, A.C.; Carvalho, P.; Vaz, F.; Lanceros-Méndez, S.; Machado, A.V.; Parreira, N.M.G.; Pierson, J.F.; Martin, N. Property Change in Multifuctional TiC_xO_y Thin Films: Effect of the O/Ti ratio. *Thin Solid Films* **2006**, *515*, 866-871.

(28) Calvillo, L.; Fittipaldi, D.; Rüdiger, C.; Agnoli, S.; Favaro M.; Valero-Vidal, C.; Di Valentin[b], C.; Vittadini, A.; Bozzolo, N.; Jacomet, S.; Gregoratti, L.; Kunze-Liebhäuser, J.; Pacchioni, G.; Granozzi G. Carbothermal Transformation of TiO_2 into TiO_xC_y in UHV: Tracking Intrinsic Chemical Stabilities. *J.Phys. Chem. C* **2014**, *118*, 22601-22610.

(29) Greeley, R.S. Electromotive Force Studies in Aqueous Solutions at Elevated Temperatures. I. The Standard Potential of the Silver-Silver Chloride Electrode. *J. Phys. Chemistry* 1960, *64*, 652-657.

(30) García, G.; Silva-Chong, J.A.; Guillén-Villafuerte, O.; Rodríguez, J.L.; González, E.R.; Pastor E. CO Tolerant Catalysts for PEM Fuel Cells: Spectroelectrochemical Studies. *Catal. Today* **2006**, *116*, 415-421.

(31) Cui, X.; Jiang, Z.; Cyclic Voltammetry and AC impedance Behavior of TiO_2 Electrodes under UV Illumination, *J. Chin. Chem. Soc.* **2003**, *50*, 1003-1008.

(32) Baez, V.B.; Graves, J.E.; Pletcher, D. The Reduction of Oxygen on Titanium Oxide Electrodes, *J. Electroanal. Chem*. **1992**, *340*, 273-286.

(33) Peláez-Abelán, E.; Rocha-Sousa, L.; Muller, W.-D.; Guastaldi, A.C. Electrochemical Stability of Anodic Titanium Oxide Films Grown at Potentials Higher than 3 V in a Simulated Physiological Solution, *Corros. Sci*. **2007**, *49*, 1645-1655.

(34) Cowling, R.D.; Hintermann, H.E. The Corrosion of Titanium Carbide, *J. Electrochem. Soc.: Electrochem. Tech.*, **1970**, *117*, 1447-1449.

(35) Beverskog, B.; Carlsson, J.O.; Delblanc Bauer, A.; Deshpandey C.V.; Doerr, H.J.; Bunshah, R.F.; O'Brien., B.P. Corrosion Properties of TiC Films Prepared by Activated Reactive Evaporation, *Surf. Coatings Tech*., **1990**, *41*, 221-229.

(36) Macdonald. D.D. The Point Defect Model for the Passive State. *J. Electrochem. Soc*. **1992**, *139*, 3434-3449.

(37) Carchini, G.; López, N. Adsorption of Small Mono- and Poly-Alcohols on Rutile TiO_2: A Density Functional Theory Study, *Phys. Chem. Chem. Phys*. **2014**, *16*, 14750-14760.

(38) Nørskov J.K.; Rossmeisl, J.; Logadottir, A.; Lindqvist, L.; Kitchin, J.R.; Bligaard, T.; Jonsson H. Origin of the Overpotential for Oxygen Reduction at a Fuel-Cell Cathode. *J. Phys. Chem. B* **2004**, *108*, 17886–17892.

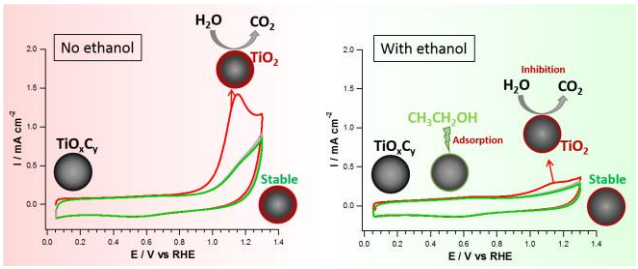
No ethanol
H_2O
CO_2
TiO_2
TiO_xC_y
Stable
I / mA cm^{-2}
E / V vs RHE
With ethanol
Inhibition
H_2O
CO_2
CH_3CH_2OH
Adsorption
TiO_xC_y
TiO_2
Stable
I / mA cm^{-2}
E / V vs RHE